Inorganic Chemistry

Article

pubs.acs.org/IC

# Extreme Differences in Oxidation States: Synthesis and Structural Analysis of the Germanide Oxometallates $A_{10}[Ge_9]_2[WO_4]$ As Well As $A_{10+x}[Ge_9]_2[W_{1-x}Nb_xO_4]$ with A = K and Rb Containing $[Ge_9]^{4-}$ Polyanions

Viktor Hlukhyy,[†] Thomas F. Fässler,*[,†] Siméon Ponou,[‡] Sven Lidin,[‡] Natalia P. Ivleva,[§] and Reinhard Niessner[§]

[†]Departement Chemie, Technische Universität München, Lichtenbergstr. 4, 85747 Garching, Germany

[‡]Polymer and Materials Chemistry, POB 124 221 00 Lund, Sweden

[§]Chair for Analytical Chemistry, Institute of Hydrochemistry, Technische Universität München, Marchioninistr. 17, 81377 Munich, Germany

Supporting Information

**ABSTRACT:** Semitransparent dark-red or ruby-red moisture- and air-sensitive single crystals of $A_{10+x}[Ge_9]_2[W_{1-x}Nb_xO_4]$ (A = K, Rb; $x$ = 0, 0.35) were obtained by high-temperature solid-state reactions. The crystal structure of the compounds was determined by single-crystal X-ray diffraction experiments. They crystallize in a new structure type ($P2_1/c$, $Z$ = 4) with $a$ = 13.908(1) Å, $b$ = 15.909(1) Å, $c$ = 17.383(1) Å, and $\beta$ = 90.050(6)° for $K_{10.35(1)}[Ge_9]_2[W_{0.65(1)}Nb_{0.35(1)}O_4]$; $a$ = 14.361(3) Å, $b$ = 16.356(3) Å, $c$ = 17.839(4) Å, and $\beta$ = 90.01(3)° for $Rb_{10.35(1)}[Ge_9]_2[W_{0.65(1)}Nb_{0.35(1)}O_4]$; $a$ = 13.8979(2) Å, $b$ = 15.5390(3) Å, $c$ = 17.4007(3) Å, and $\beta$ = 90.188(1)° for $K_{10}[Ge_9]_2WO_4$; and $a$ = 14.3230(7) Å, $b$ = 15.9060(9) Å, $c$ = 17.8634(9) Å, and $\beta$ = 90.078(4)° for $Rb_{10}[Ge_9]_2WO_4$. The compounds contain discrete $Ge_9^{4-}$ Wade's *nido* clusters and $WO_4^{2-}$ (or $NbO_4^{3-}$) anions, which are packed according to a hierarchical atom-to-cluster replacement of the $Al_2Cu$ prototype and are separated by K and Rb cations, respectively. The alkali metal atoms occupy the corresponding tetrahedral sites of the $Al_2Cu$ prototype. The amount of the alkali metal atoms on these diamagnetic compounds corresponds directly to the amount of W substituted by Nb. Thus, the transition metals W and Nb appear with oxidation numbers +6 and +5, respectively, in the vicinity of a $[Ge_9]^{4-}$ polyanion. The crystals of the mixed salts were further characterized by Raman spectroscopy. The Raman data are in good agreement with the results from the X-ray structural analyses.

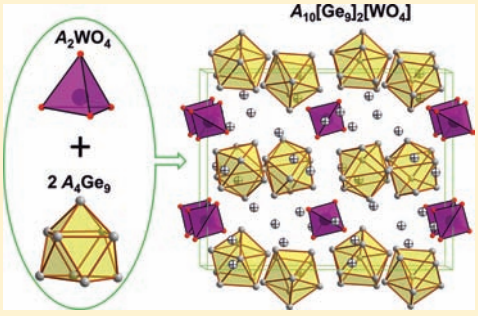


## INTRODUCTION

The multifunctionality of a material is a hot topic in contemporary materials science, because it provides unique possibilities to design novel materials that combine various physical properties in the same crystal lattice.[1] One possible approach to multifunctional materials is to prepare hybrid solids built up by the intergrowth of two networks where each network furnishes distinct properties to the solid.[1−3] Accordingly, the mixed salts that are formed by two or more types of salt-like compounds, e.g., a semiconducting Zintl phase and an insulating classical salt, are examples for pure inorganic composite materials.[4−8] Recently, the synthesis of rather unpredictable tetrelide−tetrelate compounds in which the same group 14 element coexists in a negative and a positive oxidation state in the two different anions of the structure was reported, and this marked the real breakthrough in this emerging class of metalide−metalate composite materials.[8] These tetrelide−tetrelate compounds contain the ubiquitous Zintl anions $[E_4]^{4-}$ (E = Si, Ge) and silicate anions, including the previously unknown silicate $[Si_6O_{17}]^{10-}$ built up by two condensed cyclo-trisilicate rings. Rare examples of solids that contain an element in both positive and negative oxidation states are also found in the auride−aurate series $[AAu]_n[A_3AuO_2]$ (A = Rb, Cs).[9] The next logical step was to look for double salts with the larger Zintl anions $[E_9]^{4-}$ which can be regarded as small charged element particles that open new possibilities for chemical reactions and the development of nanoscaled materials.[10−13] In fact, these anions can be functionalized and interconnected through controlled oxidation, thereby allowing an effective tuning of cluster size and properties.[14−17]

On the other hand, the existence of the tetrelide−tetrelate hybrid compounds also suggests the availability of unprecedented types of pure inorganic multifunctional materials involving Zintl phases and transition metal oxides. Among

Received: October 25, 2011
Published: March 12, 2012

   dx.doi.org/10.1021/ic202234b | Inorg. Chem. 2012, 51, 4058−4065

Table 1. Crystal Data and Structure Refinement of $A_{10+x}Ge_{18}W_{1-x}Nb_xO_4$ Compounds (Space Group $P2_1/c$, $Z = 4$, GeB-Non-Split Average Model)

| compound | 1 | 2 | 3 | 4 |
|---|---|---|---|---|
| empirical formula | $K_{10.35(1)}Ge_{18}W_{0.65(1)}Nb_{0.35(1)}O_4$ | $Rb_{10.35(1)}Ge_{18}W_{0.65(1)}Nb_{0.35(1)}O_4$ | $K_{10}Ge_{18}WO_4$ | $Rb_{10}Ge_{18}WO_4$ |
| $M_w$, g mol$^{-1}$ | 1927.07 | 2407.26 | 1945.47 | 2409.17 |
| $T$, K | 293 | 293 | 150 | 150 |
| $a$, Å | 13.908(1) | 14.361(3) | 13.8979(2) | 14.3230(7) |
| $b$, Å | 15.909(1) | 16.356(3) | 15.5390(3) | 15.9060(9) |
| $c$, Å | 17.383(1) | 17.839(4) | 17.4007(3) | 17.8634(9) |
| $\beta$, deg | 90.050(6) | 90.01(3) | 90.188(1) | 90.078(4) |
| $V$, Å$^3$ | 3846.0(5) | 4190.3(15) | 3757.8(1) | 4069.7(4) |
| $\mu$ (Mo K$\alpha$), mm$^{-1}$ | 17.0 | 26.5 | 18.3 | 27.8 |
| $\rho$, g cm$^{-3}$ | 3.33 | 3.82 | 3.44 | 3.93 |
| diffractometer | Oxford-Xcalibur3 | Stoe IPDS-2T | Oxford-Xcalibur3 | Oxford-Xcalibur3 |
| $F(000)$ | 3478 | 4214 | 3488 | 4208 |
| cryst size (mm$^3$) | 0.25 × 0.15 × 0.10 | 0.30 × 0.10 × 0.10 | 0.30 × 0.30 × 0.20 | 0.24 × 0.22 × 0.18 |
| $\theta$ range for data collection (deg) | 3.47 − 20.30 | 3.30 − 23.73 | 3.00 − 27.50 | 2.93 − 25.00 |
| index ranges | $-13 \le h \le 10$; ±15; ±16 | $-16 \le h \le 15$; ±18; ±20 | $-18 \le h \le 17$; ±20; $-22 \le l \le 19$ | ±17; ±18; $0 \le l \le 21$ |
| reflns collected | 15358 | 27051 | 58947 | 14274 |
| independent reflns | 3726 | 6255 | 8616 | 7157 |
| reflns with $I \ge 2\sigma(I)$ | 3251 | 4726 | 7790 | 4318 |
| data/params | 3726/301 | 6255/282 | 8616/300 | 7157/280 |
| GOF on $F^2$ | 1.069 | 1.079 | 1.039 | 1.019 |
| $R_1$, $wR_2$ $[I \ge 2\sigma(I)]$ | 0.065, 0.159 | 0.112, 0.267 | 0.083, 0.215 | 0.116, 0.270 |
| $R_1$, $wR_2$ (all data)[a,b] | 0.073, 0.165 | 0.139, 0.290 | 0.088, 0.219 | 0.161, 0.295 |
| largest diff. peak and hole (e Å$^{-3}$) | 2.09 and −1.40 | 3.25 and −4.30 | 5.71 and −3.45 | 4.60 and −2.00 |

[a] $R_1 = \sum||F_c| - |F_c||/\sum|F_o|$; $wR_2 = [\sum[w(F_o^2 - F_c^2)2]/\sum[w(F_o^2)^2]]^{1/2}$. [b] $w = 1/[\sigma^2(F_o^2) + (aP)2 + bP]$, where $P = (\mathrm{Max}(F_o^2,0) + 2F_c^2)/3$.

the numerous semiconducting transition metal oxides, the tungsten and niobium oxides are of particular interest and have been investigated extensively for their excellent optical properties which form the basis of their wide use as phosphors, solid-state laser materials, scintillation detectors, and optoelectronic devices.[17−20]

Thus, the germanide−oxometallate mixed salts may combine the semiconducting properties of the germanide with the outstanding optical properties of the tungstate/niobate, and this may lead to interesting electro-optical properties with a high potential for technological applications. The combination of alkali metal tungstates $A_2WO_4$ with the Zintl phases $A_4Ge_9$ (A = K, Rb) that contain a $Ge_9^{4-}$ *nido* cluster, led to a new type of composite material.

Herein, we describe the synthesis in Nb containers and the crystal structures of the composite compounds $A_{10.35}[Ge_9]_2[W_{0.65}Nb_{0.35}O_4]$ (A = K and Rb) in which the *nido* cluster $Ge_9^{4-}$ and the anion $[MO_4]^{(2+x)-}$ (M = $W_{1-x}Nb_x$) coexist in the crystal lattice of an intergrowth structure. The structures of niobium-free samples $A_{10}[Ge_9]_2[WO_4]$ (A = K and Rb) reveal a lower amount of alkali metal atoms in the compounds. The synthesis of the extremely air-sensitive deep-red or ruby-red rod-like single crystals of the title compounds proceeded in a high-temperature reaction in sealed crucibles in good yields.

## EXPERIMENTAL SECTION

**Syntheses.** All manipulations were performed in an argon-filled glovebox with moisture and $O_2$ levels lower than 1 ppm. The reactants were elemental K (Merck, 99%), Rb (Riedel-de-Haën, 99.9%), Ge (Chempur, 99.9999+ %), and W (Chempur, 99.95%) and $WO_3$ (Aldrich, 99+ %), $K_2WO_4$ (Chempur, 99.9%), $Rb_2WO_4$ (Chempur, 99.9%), $GeO_2$ (Aldrich, 99.999%), and HgO (Alfa Aesar, 99.0%). The solids were weighed and loaded in Nb crucibles (Osnabruegge, 99.9%) or in an Nb ampule with an inner corundum crucible, which were weld-sealed on both sides and jacketed in a fused silica Schlenk tube under argon and evacuated to prevent oxidation of the crucibles at high temperatures.

(i) Mixtures of alkali metal and Ge as well as oxides $WO_3$ and HgO in the ratio A/Ge/$WO_3$/HgO = 5:5:1:1 were heated in sealed Nb crucibles at a rate of 120 °C/h first to 600 °C, kept at this temperature for 24 h, then heated to 800 °C, kept for 120 h, and subsequently cooled to room temperature at a rate of 6 °C/h. HgO was used as an oxygen donor. By this procedure, ruby-red transparent rod-shaped single crystals of $K_{10+x}[Ge_9]_2[W_{1-x}Nb_xO_4]$ were obtained. An A/Ge ratio close to 1 used for the starting mixtures turned out to be important in order to achieve a good crystal quality of the desired phase. (ii) Alternatively, mixtures of elemental K (or Rb), Ge, and W with $GeO_2$ in the ratio A/Ge/W/$GeO_2$ = 5:3:1:2 were heated and treated in a similar way as described in i. This route led to single crystals of $Rb_{10+x}[Ge_9]_2[W_{1-x}Nb_xO_4]$. (iii) $K_{10+x}[Ge_9]_2[W_{1-x}Nb_xO_4]$ can also be obtained by heating of a mixture of the composition K/Ge/$K_2WO_4$/Nb = 8:18:1:2 in sealed niobium crucibles in an induction furnace (Hüttinger Elektronik, Freiburg, Typ TIG 2.5/300). The mixture was first heated under flowing argon to approximately 940 °C and kept at this temperature for 1 h. After the melting procedure, the sample was slowly cooled to approximately 650 °C, kept at this temperature for 1 h, and finally cooled to room temperature within 30 min. However, the induction melting resulted in crystals of poor quality, although the "mixed salt" was detected as the main phase in the powder diffractogram. (iv) Single crystals of the "Nb-free" double salts $A_{10}[Ge_9]_2WO_4$ (A = K, Rb) were obtained directly from the parent compounds $A_4Ge_9$ and $A_2WO_4$ (A = K, Rb) by heating in sealed niobium ampules with an inner corundum crucible using the following thermal treatment: the samples were first heated in a muffle furnace to 950 °C and kept at this temperature for 12 h. Next, the temperature was lowered at a rate of 6 °C/h to 650 °C, and this temperature was kept for 120 h before the sample was quenched in the air. However, the crystals of the Rb-based phases were of rather poor quality compared to those of the K analogs.


dx.doi.org/10.1021/ic202234b | Inorg. Chem. 2012, 51, 4058−4065

Table 2. Unit Cell Parameters[a] of the $A_{10+x}Ge_{18}W_{1-x}Nb_xO_4$ ($Z = 4$) Compounds at 293 K and Corresponding Volumes of the Parent Compounds

| A | $x$ | $a$/Å | $b$/Å | $c$/Å | $\beta$/deg | $V$/Å$^3$ | $8 \times V(A_4Ge_9) + 4 \times V(A_yMO_4)$/Å$^3$ [b] |
|---|---|---|---|---|---|---|---|
| K | 0.35(1) | 13.908(1) | 15.909(1) | 17.383(1) | 90.05(1) | 3846.0(5) (sc) | 3824 |
| | | 13.924(1) | 15.901(2) | 17.418(2) | 90.113(8) | 3856.5(7) (p) | |
| K | 0 | 13.955(1) | 15.663(2) | 17.501(2) | 90.144(7) | 3825.2(6) (sc) | 3772 |
| | | 13.941(1) | 15.643(1) | 17.473(1) | 90.277(4) | 3810.4(4) (p) | |
| Rb | 0.35(1) | 14.361(3) | 16.356(3) | 17.739(4) | 90.01(3) | 4190.2(2) (sc) | |
| Rb | 0 | 14.382(1) | 16.044(1) | 17.894(1) | 90.230(7) | 4128.8(6) (p) | 4108 |

[a](sc) single crystal data, (p) powder data. [b]The lattice parameters of $K_3WO_4$, $Rb_3WO_4$, $K_4Ge_9$, and $Rb_4Ge_9$ are taken from ICSD database,[29] whereas those of $K_3NbO_4$ are taken from the International Centre for Diffraction Data (ICDD) database (PDF 02-052-1895). No evidence for the existence of $Rb_3NbO_4$ has been found.

**Single-Crystal Structure Determination.** Semitransparent dark-red or ruby-red, rod-shaped single crystals were selected and mounted on top of a glass fiber. Intensity data were collected on an Oxford XCalibur3 CCD area-detector diffractometer ($K_{10+x}[Ge_9]_2W_{1-x}Nb_xO_4$, compound **1**) and a Stoe IPDS-2T image plate diffractometer with graphite-monochromatized Mo K$\alpha$ (0.71073 Å) radiation in oscillation mode ($Rb_{10+x}[Ge_9]_2W_{1-x}Nb_xO_4$, compound **2**) at room temperature. The single crystals of $K_{10}[Ge_9]_2WO_4$ (compound **3**) and $Rb_{10}[Ge_9]_2WO_4$ (compound **4**) were measured at 150 K on an Oxford XCalibur3 CCD area-detector diffractometer. Numerical absorption corrections were applied to the data sets (X–Shape/X–Red).[21] All relevant crystallographic data for the data collection and refinement procedures are listed in Table 1.

At first, the structure of $K_{10.35(1)}Ge_{18}W_{0.65(1)}Nb_{0.35(1)}O_4$ (**1**) was solved, and its structure model was then used as a starting model for the structure refinement of compounds **2**, **3**, and **4**. Although the unit cell angles are all close to 90°, the structure of $K_{10.35(1)}Ge_{18}W_{0.65(1)}Nb_{0.35(1)}O_4$ was solved in the monoclinic space group $P2_1/c$ using the Patterson method, which allowed the localization of the heavy atoms W/Nb (M) and most of the Ge atoms.[22] The positions of the remaining Ge and K atoms were determined through difference Fourier syntheses. All atoms were refined with anisotropic displacement parameters. The O positions were localized in residual electron density maps around the M position. One out of two $Ge_9$ clusters in the structure is disordered. The K atoms with the largest displacement ellipsoids are located within the layer of the disordered cluster (**B**), indicating a correlation with the disorder of this cluster.

The refinement based on the nonsplit average model for $Ge_9$ clusters was at first unsatisfactory with a high residual $R_1$ of about 25%. However, the monoclinic cell is pseudo-orthorhombic with a $\beta$ angle of 90.05°, and thus this is a typical case of twinning by pseudomerohedry, known to occur when the lattice of the individual has a metric close to that of a higher holohedry. The appropriate twinning matrix was found to be −1 0 0, 0 1 0, 0 0 1, which allowed for a lowering of the residuals to an acceptable level. According to large ADP values for the W positions, a mixing of $W^{6+}/Nb^{5+}$ with a ratio of 0.67(1):0.33(1) was assumed. The results of an EDX analysis as well as Raman data (for compound **3**) confirm the presence of small amounts of Nb in the samples.

The atom K11 with a site occupancy of ~40% is situated at a distance of 2.81 Å beside K10 with a largely elongated displacement ellipsoid. Therefore, the further structure refinement was performed by using a split-atom model for K10 (K10A and K10B), averaged isotropic displacement parameters for the atoms K11/K10A/K10B, correlation between their occupancies, and $W^{6+}/Nb^{5+}$ mixing in the $[W_{1-x}Nb_xO_4]^{(2+x)-}$ tetrahedra. Calculated occupancies of 0.35(1)/0.65(1)/0.35(1) for K11/K10A/K10B and 0.65(1)/0.35(1) for W/Nb result in the overall chemical formula $K_{10.35(1)}{}^{+}[Ge_9{}^{4-}]_2[W_{0.65(1)}Nb_{0.35(1)}O_4]^{2.35-}$. The possible models of alternating groups of corresponding K atoms with reasonable K–K distances and a shortest periodicity are shown in Figure S1 (Supporting Information). For this model, the final residuals were $R_1 = 0.073$ and $wR_2 = 0.165$ for all data and $R_1 = 0.065$ and $wR_2 = 0.159$, for observed reflections [$I \geq 2\sigma(I)$] (structure model **1a**). The positional parameters and interatomic distances for the structure model **1a** of $K_{10.35(1)}[Ge_9]_2[W_{0.65(1)}Nb_{0.35(1)}O_4]$ are listed in Tables S2 and S3 (Supporting Information).

Finally, the split-atom model for five Ge atoms with the largest ADP values of the disordered $Ge_9$ cluster **B** was applied in the structure refinement using the averaged values of their isotropic displacement parameters and a restraint for one Ge–Ge bond length. In this case, the residuals increased to $R_1 = 0.083$ and $wR_2 = 0.188$ for all data (structure model **1b**, Table S4). Such a split-atom model was successfully used to describe the orientational disorder of the $Ge_9$ cluster in the parent compound $K_4Ge_9$.[26] Interestingly, the second cluster in $K_4Ge_9$ is ordered as it is in the mixed salts $A_{10+x}[Ge_9]_2[MO_4]$ (cluster **A**). It is necessary to note that a careful exploration of the reciprocal space in order to detect any additional scattering features revealed no classical superstructure reflections or incommensurate satellites, which would indicate an ordering of the split atomic groups described.

Similarly, the crystal structure of compound **3** was refined (Supporting Information: Tables S5–S6). Only 10 atomic positions for K atoms were found, all fully occupied, resulting in the formula $K_{10}{}^{+}[Ge_9{}^{4-}]_2[WO_4]^{2-}$. Ten peaks with the highest values in the residual density map are situated close to the atoms of the disordered $Ge_9$ cluster **B**, indicating the superposition of more than two conformations of cluster **B**. However, no appropriate split-atom model for this $Ge_9$ cluster was found to be adequate to describe such a pronounced orientational disorder. Thus, for the nonsplit average model, the final residuals when applying the twinning law were $R_1 = 0.089$ and $wR_2 = 0.219$ for all data and $R_1 = 0.083$ and $wR_2 = 0.215$ for observed reflections [$I \geq 2\sigma(I)$].

In a similar way, the crystal structures of Rb compounds **2** and **4** were refined, resulting in formulas $Rb_{10.35(1)}{}^{+}[Ge_9{}^{4-}]_2[W_{0.65(1)}Nb_{0.35(1)}O_4]^{2.35-}$ and $Rb_{10}{}^{+}[Ge_9{}^{4-}]_2[WO_4]^{2-}$, respectively (Supporting Information: Tables S7–S12). Split-atom models were used to describe the orientational disordering of $Ge_9$ clusters **B** for both compounds (**2** and **4**) as well as a correlation between $W^{6+}/Nb^{5+}$ mixing and split-atom occupancy Rb11/Rb10A/Rb10B for compound **2**. As already mentioned, the crystals of the Rb-based phases were of lower quality, resulting in higher final residuals.

**Powder X-Ray Diffraction.** The powder diffractograms were collected in Debye-Scherer geometry on a STOE STADI P2 powder diffractometer (Ge(111) monochromator for Cu K$\alpha_1$ radiation: $\lambda$ = 1.54056 Å) equipped with a linear position-sensitive detector PSD. The powder diffractograms showed that except for the main phase the samples of $K_{10+x}[Ge_9]_2[W_{1-x}Nb_x]O_4$ (**1**) and $Rb_{10+x}[Ge_9]_2[W_{1-x}Nb_x]O_4$ (**2**) contained small amounts of $K_2WO_4$ and $Rb_2WO_4$, respectively, while the samples of $K_{10}[Ge_9]_2WO_4$ (**3**) and $Rb_{10}[Ge_9]_2WO_4$ (**4**) contained only minor amounts of elemental W or Ge, respectively (Figures S2 and S3). The unit cell parameters at room temperature for $A_{10+x}Ge_{18}W_{1-x}Nb_xO_4$ (A = K, Rb) are listed in Table 2. Chemical compositions of the single crystals extracted from the reaction products were investigated with a JEOL-SEM 5900LV scanning electron microscope equipped with an integrated energy dispersive X-ray system and a LINK AN 10000 detector system for EDX analysis. A quantitative estimate of the atomic ratio was difficult to perform due to


dx.doi.org/10.1021/ic202234b | Inorg. Chem. 2012, 51, 4058–4065

the extreme sensitivity of the compounds to air and moisture. However, an atomic ratio of A/Ge close to 1:2 (A = K, Rb) was observed for most of the analyzed crystals, as well as Ge/W or Ge/(W +Nb) atomic ratios close to or larger than 10:1.

**Raman Spectroscopy.** The Raman spectrum of a single crystal of $Rb_{10+x}Ge_{18}W_{1-x}Nb_xO_4$, sealed in a 1 mm Ø glass capillary, with a 0.01 mm wall thickness, was recorded at room temperature with a Bio-Rad Fourier transform Raman system, employing the 1024 nm radiation of an infrared Nd:YAG laser. The notchfilter cut the signal for wave numbers <130 $cm^{-1}$. A LabRAM HR Raman microscope system with a 785 nm excitation wavelength for the laser diode, a Raman edge filter (<50 $cm^{-1}$), and 10 × objectives (NA 0.25) were used for the measurement of $K_{10}Ge_{18}WO_4$ and $Rb_{10}Ge_{18}WO_4$ single crystals (sealed in a 0.3 mm Ø glass capillary, 0.01 mm wall thickness). At least three measurements were carried out on different crystals in each case, and the results were highly reproducible.

**Magnetic Measurements.** The magnetic measurements on crystals mechanically separated from the crushed products were carried out on a MPMS XL5 SQUID magnetometer (Quantum Design).

## RESULTS AND DISCUSSION

**Crystal Structure Description.** Compounds **1**, **2**, **3**, and **4** crystallize in a new structure type in the space group $P2_1/c$. The crystal structure of $K_{10}[Ge_9]_2WO_4$ is depicted in Figure 1. It

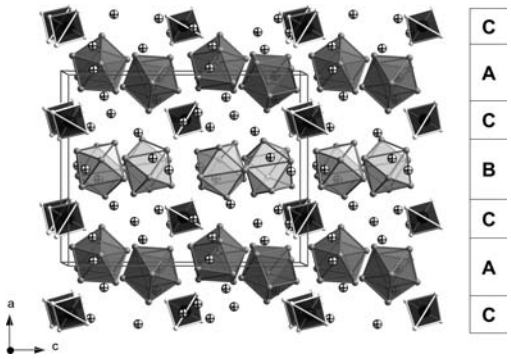


**Figure 1.** Projection of the structure of $K_{10}[Ge_9]_2WO_4$ along the *b* axis showing alternating layers of germanide (**A** and **B**) and oxometallate (**C**) with the sequence **CACBCAC**. The $WO_4^{2-}$ anions are shown as black polyhedra. The gray spheres are Ge atoms in the $Ge_9$ clusters (gray, clusters **A**; white, clusters **B**), and isolated crossed spheres are $K^+$ cations.

contains two crystallographically independent $Ge_9$ clusters (**A** and **B**) and tetrahedral oxo-bonded anions $WO_4^{2-}$ (**C**), which are separated by K atoms. The three anion types in compounds **1**−**4** occur in separate layers propagating in the *bc* plane. Whereas the $MO_4$ tetrahedra and the $Ge_9$ clusters **A** are ordered in all cases, clusters **B** are disordered.

In $A_{10+x}[Ge_9]_2[MO_4]$ (A = K, Rb, M = Nb/W), the transition metal position (M) is statistically occupied by W and Nb with the latter stemming from the crucible used for the synthesis. The presence of the elements A, Ge, Nb, and W is also shown by analyzing the crystals after the X-ray diffraction data collection by EDX. The mixing of tetrahedral $WO_4^{2-}$ and $NbO_4^{3-}$ units ($W^{6+}$ and $Nb^{5+}$, respectively) to give a statistical composition of $[W_{1-x}Nb_xO_4]^{(2+x)-}$ leads to an increase of the negative charge, which is counterbalanced by one additional K or Rb atom per $NbO_4^{3-}$ unit, resulting in the formula $A_{10.35}[Ge_9]_2[W_{0.65}Nb_{0.35}O_4]$. The possible alternative, namely the presence of paramagnetic $Ge_9^{3-}$ anions[23] according to $A_{10+x}^{+}[Ge_9^{4-}]_2][W_{1-x}Nb_xO_4]^{(2+x)-}$, can be ruled out by magnetic measurements, which show diamagnetic properties for A = K.

Cluster **A** is ordered and displays the expected shape[13] of an idealized $C_{4v}$-symmetric monocapped square antiprismatic polyhedron. Cluster **B** is disordered, resulting in rather large anisotropic displacement parameters (ADPs) for some of the Ge atoms. Such distortions due to orientational disorder are very common in structures featuring $E_9$ *nido* clusters such as $K_4Ge_9$, $Na_{12}Ge_{17}$, $Rb_{12}Sn_{17}$, $K_{52}Sn_{82}$, $Cs_{52}Sn_{82}$, $K_4Pb_9$, and $Rb_4Pb_9$.[24,25]

Considering the idealized $C_{4v}$ symmetry for cluster **A**, the intracluster Ge−Ge contacts between the atoms with almost equivalent positions and similar bond lengths can be classified into four groups (Supporting Information: Figure S4, Table S1): the distances to the capping Ge1 atom (group **I**), the distances between Ge atoms within the capped square (group **II**), the distances between the Ge atoms of the two almost coplanar squares (group **III**), and finally the distances between the atoms of the open basal square (group **IV**). In fact, there are only two types of effective bond lengths in clusters **A** (ordered). The distances of groups **I**, **III**, and **IV** between the Ge atoms are shorter, ranging from 2.52(1) Å to 2.62(1) Å for $K_{10.35}[Ge_9]_2[W_{0.65}Nb_{0.35}O_4]$ (**1**), 2.53(1) Å to 2.63(1) Å for $Rb_{10.35}[Ge_9]_2[W_{0.65}Nb_{0.35}O_4]$ (**2**), 2.52(1) Å to 2.64(1) Å for $K_{10}[Ge_9]_2[WO_4]$ (**3**), and 2.54(1) Å to 2.65(1) Å for $Rb_{10}[Ge_9]_2[WO_4]$ (**4**), than those of group **II** between five-bonded atoms that range from 2.70(1) Å to 3.01(1) Å for **1**, 2.72(1) Å to 2.97(1) Å for **2**, 2.69(1) Å to 3.03(1) Å for **3**, and 2.73(1) Å to 2.97(1) Å for **4**. This corresponds to the bonding pattern found for all isolated $Ge_9$ *nido* clusters. Similar bond length distributions are observed in the ordered $Ge_9^{4-}$ cluster of

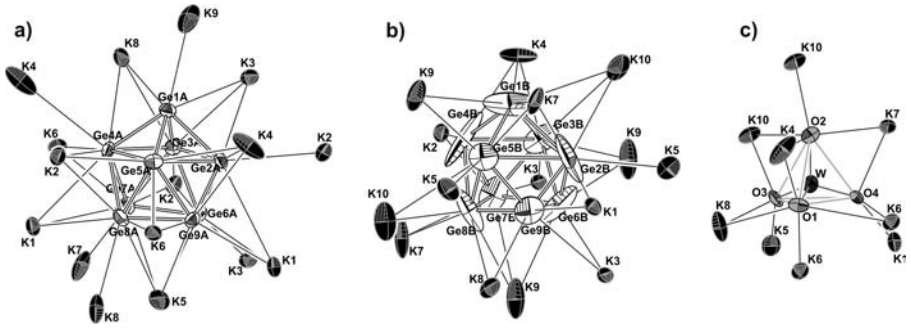


**Figure 2.** View of the coordination of the polyanions in $K_{10}[Ge_9]_2[WO_4]$ by the closest $K^+$ cations. (a) $Ge_9^{4-}$ cluster **A**, (b) $Ge_9^{4-}$ cluster **B**, (c) $WO_4^{2-}$. The displacement ellipsoids are shown at the 50% probability level. The K, Ge, W, and O atoms are drawn in black, white, dark gray, and gray, respectively.


dx.doi.org/10.1021/ic202234b | *Inorg. Chem.* 2012, 51, 4058−4065

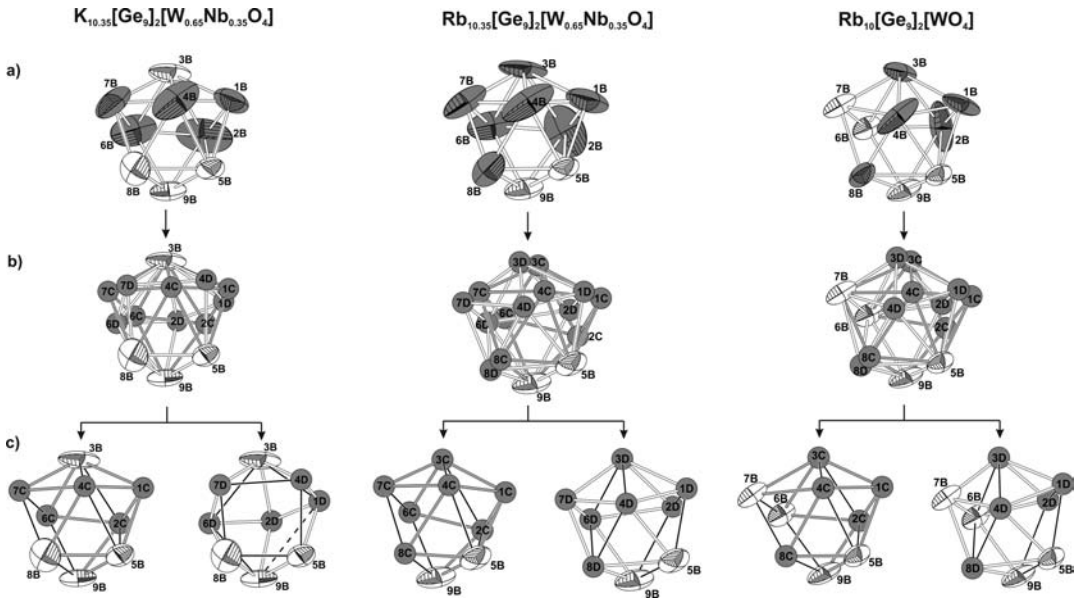


**Figure 3.** Representation of the disordered $Ge_9$ clusters **B** (row a), the corresponding models with split positions of various atoms of these clusters (row b), and structure models with two ordered variants (row c) in $K_{10.35}[Ge_9]_2[W_{0.65}Nb_{0.35}O_4]$, $Rb_{10.35}[Ge_9]_2[W_{0.35}Nb_{0.35}O_4]$, and $Rb_{10}[Ge_9]_2[WO_4]$. The 3B, 5B, 8B, and 9B positions (white) in $K_{10.35}[Ge_9]_2[W_{0.65}Nb_{0.35}O_4]$; the 5B and 9B positions in $Rb_{10.35}[Ge_9]_2[W_{0.65}Nb_{0.35}O_4]$; as well as the 5B, 6B, 7B, and 9B positions in $Rb_{10}[Ge_9]_2[WO_4]$ are congruent in both orientations shown in row c. All displacement ellipsoids are shown at the 50% probability level. In row c, square antiprisms are emphasized.

the binary phase $K_4Ge_9$,[24] with Ge−Ge distances ranging from 2.52 Å to 2.91 Å as well as in the $Cs_4Ge_9$ homologue (2.52−3.01 Å).[26]

The bond lengths in the disordered clusters **B** are roughly in the same range and lie between 2.35(1) Å and 3.10(1) Å in $K_{10.35}[Ge_9]_2[W_{0.65}Nb_{0.35}O_4]$ (**1**), 2.47(2) Å and 3.03(2) Å in $Rb_{10.35}[Ge_9]_2[W_{0.65}Nb_{0.35}O_4]$ (**2**), 2.33(1) Å and 3.19(1) Å in $K_{10}[Ge_9]_2[WO_4]$ (**3**), and 2.51(1) Å and 3.18(1) Å in $Rb_{10}[Ge_9]_2[WO_4]$ (**4**), but because of the strong distortion, the usually observed bonding pattern of an $E_9$ *nido* cluster cannot be rigorously confirmed and must not be discussed in further detail.

The distortion of the clusters from ideal $C_{4v}$ symmetry can be assessed by the ratio of the two diagonals ($d_1$ and $d_2$) of the open basal square, which should be equal to 1 in an ideal geometry. Clusters **A** with a $d_1/d_2$ ratio of 1.08−1.10 and a dihedral angle $\alpha$ of 6.3−7.7° (180°, cap-to-cap fold angle) in the mixed salts have the shape of a distorted monocapped square antiprism with a symmetry close to $C_{2v}$. Clusters **B** ($d_1/d_2$ = 1.15−1.24 and $\alpha$ of 10.1−17.8°) are more distorted, which is attributed to the mixing of two (or more) configurations of the clusters in the averaged model.

The large anisotropic electron density around five of the nine atom positions of clusters **B** in $K_{10+x}[Ge_9]_2[W_{1-x}Nb_xO_4]$ (**1**) and $Rb_{10}[Ge_9]_2[WO_4]$ (**4**) and seven of nine positions in $Rb_{10+x}[Ge_9]_2[W_{1-x}Nb_xO_4]$ (**2**) is better described by a superposition of two clusters **C** and **D** (Figure 2, Table S1) with different orientations with respect to the underlying square antiprism. They appear with **C**/**D** ratios of 69:31, 41:59, and 54:46 for **1**, **4**, and **2**, respectively. Clusters **C** are less distorted than the averaged model of cluster **B** (disordered) and have the shape of an almost $C_{2v}$-symmetric, distorted monocapped square antiprism, with $d_1/d_2$ ratios of 1.12, 1.08, and 1.16 and dihedral angles $\alpha$ of 8.3°, 7.1°, and 7.6° for **1**, **2**, and **4**, respectively. The Ge−Ge intracluster distances in clusters **C** range from 2.45(2) Å to 2.97(2), from 2.36(2) Å to 2.89(2), and from 2.33(2) Å to 3.07(2) Å in **1**, **2**, and **4**, respectively.

Clusters **D** are more distorted than clusters **B**. The cluster **D** in compound **1** contains one additional tetragonal face, whereas in those of compounds **2** and **4** the corresponding $d_1/d_2$ ratios of 1.34 and 1.22 and dihedral angles $\alpha$ of 24.7° and 17.6° indicate a significant distortion from the monocapped square-antiprismatic shape toward a tricapped trigonal-prismatic geometry. As mentioned in the Experimental Section, no appropriate split-atom model for cluster **B** was found for $K_{10}[Ge_9]_2[WO_4]$. To unravel the disorder, a superposition of more than two orientational conformers is needed. [The ordering of $Ge_9$ clusters will be reported in a forthcoming paper for $Cs_{10}[Ge_9]_2[WO_4]$ and $Cs_{11}[Ge_9]_2[VO_4]$.[27]]

The $Ge_9$ cluster **A** in $K_{10}[Ge_9]_2[WO_4]$ is surrounded by the 16 closest $K^+$ neighbors (Figure 3a) in a way comparable to that observed in the binary phase $K_4Ge_9$ with several of the cations capping the polyhedral faces of the cluster units.[24] The $Ge_9$ cluster **B** has 15 $K^+$ neighbors (Figure 3b). The K−Ge distances for cluster **A** vary from 3.32(1) Å to 4.20(1) Å and in cluster **B** from 3.26(1) Å to 4.21(1) Å.

The oxygen atoms are positioned around the W atom in a tetrahedral coordination. The W−O distances in $K_{10}[Ge_9]_2[WO_4]$ range from 1.73(2) Å to 1.78(2) Å (at 150 K) and are close to those in $K_2WO_4$ (from 1.76 Å to 1.81 Å at 293 K).[28,29] The $WO_4^{2-}$ anions in $K_{10}[Ge_9]_2[WO_4]$ are surrounded by 9 $K^+$ cations (Figure 3c), which is less than the 11 $K^+$ neighbors found in $K_2WO_4$. The distances between the K atoms and the oxygen atoms of the anions vary from 2.55(2) Å to 3.41(2) Å in the nonsplit $K_{10}[Ge_9]_2[WO_4]$ model, which is close to those in the simple tungstate $K_2WO_4$ (from 2.68 Å and 3.20 Å). There is one additional defective K position in the coordination sphere of the $MO_4$ units in $K_{10.35}[Ge_9]_2[W_{0.65}Nb_{0.35}O_4]$ (**1**) with the closest distance of 2.80(3) Å to O2 and a distance of 2.81(3) Å to K10, which required the splitting of the K10 atom as described above


dx.doi.org/10.1021/ic202234b | *Inorg. Chem.* 2012, 51, 4058−4065

(Figure S1). The M−O distances in $K_{10.35}[Ge_9]_2[W_{0.65}Nb_{0.35}O_4]$ are in the same range (from 1.73(2) Å to 1.79(2) Å) as the ones in the Nb-free $K_{10}[Ge_9]_2[WO_4]$ double salt.

The topological analysis of the structures shows that they are hierarchical derivatives of the *initiator* $Al_2Cu$ type ($I4/mcm$)[30] with the $Ge_9$ clusters at the Al and the $[MO_4]^{(2+x)-}$ anions at the Cu positions (Figure 4), while the $A^+$ cations are located in

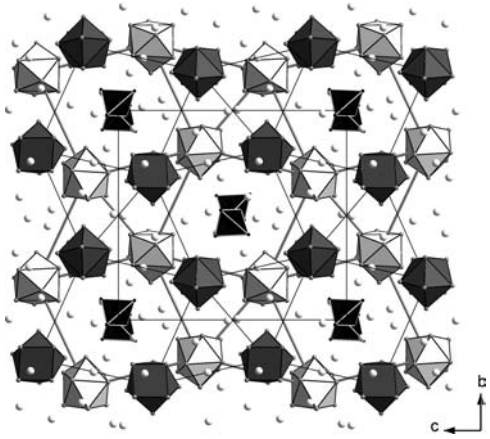

**Figure 4.** Projection of the structure of $K_{10}[Ge_9]_2[WO_4]$ along the *a* axis revealing the hierarchical replacement relation to the $Al_2Cu$ type. $Ge_9$ clusters in polyhedral representation with alternating $3^2344$ layers A (gray) and layers B (white). The $WO_4^{2-}$ anions are shown as black tetrahedra. The light-gray spheres are Ge atoms in the $Ge_9$ clusters, and isolated white spheres are $K^+$ cations.

the resulting tetrahedral voids of the structure. The relationship between the basic $Al_2Cu$ structure and the hierarchical derivative structure by atom-by-cluster replacement plus filling of 10 + *x* over 17 tetrahedral voids can be written as: $\square_{17}Al_2Cu \cong \square_{7-x}A_{10+x}[Ge_9]_2[MO_4]$ (□ denoting the tetrahedral void). As a consequence, the structures of $A_{10+x}[Ge_9]_2[W_{1-x}Nb_xO_4]$ may be described as an asymmetric stacking in the [100] direction of almost planar $3^2434$ nets (A and B) formed by isolated $Ge_9$ clusters that are separated by a larger planar $4^4$ net of oxometallate layers (C), resulting in the stacking sequence ACBC. Apart from the effect of the empty tetrahedral voids, the deformation of the formally tetragonal unit cell of the aristotype ($Al_2Cu$) to a monoclinic one is mainly a result of the site coloring due to the different orientations of the "non-spherical" $Ge_9$ clusters for a better packing in the crystal. The arrangement of the $[Ge_9]$ clusters differs clearly from that in the binary phases $A_4Ge_9$ which crystallize in a $Cr_3Si$ hierarchical derivative, showing a 3D entanglement of linear chains of clusters.

The structure of the anions and their coordination by the alkali metal cations in $K_{10}[Ge_9]_2[WO_4]$ strongly resemble those of the respective parent compounds, namely, the Zintl phases $K_4Ge_9$ and $K_2WO_4$ with a 2:1 ratio, and thus $K_{10}[Ge_9]_2[WO_4]$ can be formulated as $[K_4Ge_9]_2{\cdot}[K_2WO_4]$. Similarly the structure of $A_{10.35}[Ge_9]_2[W_{0.65}Nb_{0.35}O_4]$ can be regarded as $[A_4Ge_9]_2{\cdot}[A_2WO_4]_{0.65}{\cdot}[A_3NbO_4]_{0.35}$.

The formation of such composite materials by simply reacting two different parent compounds, namely, a binary intermetallic phase or Zintl phase $A_4Ge_9$ (with alkali metal, A, and a semimetal, Ge) and an oxo-bonded transition metal (oxide) is unpredictable. At first glance, it emphasizes the good topological compatibility of the two (or more) anions. Hence, it is likely that the main factor for the formation of these hybrid compounds is the more favorable Madelung energy compared to that of the parent compounds. However, the volume per formula unit of the composite materials at room temperature is only about 0.5−1.5% larger than the sum of the volumes of the two parent compounds (Table 2), which indicates that the interactions in these new mixed salts are similar to those in the parent compounds. A larger volume increase of about 4.2% has been observed for the tetrelide−tetralate species.[8,31] Analysis of the unit cell parameters for $A_{10+x}Ge_{18}W_{1-x}Nb_xO_4$ (A = K, Rb) measured at room temperature (Table 2) indicates an increase of the volume (increase of *b* and slight decrease of *a* and *c* parameters) upon the substitution of $A_2WO_4$ by $A_3NbO_4$, which is in accordance with the increasing cation ($K^+$ or $Rb^+$) concentration.

The differential thermal analysis (DTA) of $K_{10}[Ge_9]_2[WO_4]$ was recorded from room temperature up to 900 °C and indicates that this phase is stable over the whole temperature range (Figure S5).

**Vibrational Spectra.** The Raman spectra were recorded for compounds **2**, **3**, and **4** (Figure 5). An automatic peak search using the instrument routine resulted in the following peak positions ($cm^{-1}$): 55 ($Ge_9$), 164 ($Ge_9$), 194 ($Ge_9$), 221 ($Ge_9$) 327 ($WO_4$), and 923 ($WO_4$) for $K_{10}[Ge_9]_2[WO_4]$; 56 ($Ge_9$), 164 ($Ge_9$), 193 ($Ge_9$), 222 ($Ge_9$), 326 ($WO_4$), and 921 ($WO_4$) for $Rb_{10}[Ge_9]_2[WO_4]$; and 325 ($WO_4$, $NbO_4$), 807 ($NbO_4$), 916 ($WO_4$), 164 ($Ge_9$), and 221 ($Ge_9$) for $Rb_{10.35}[Ge_9]_2[W_{0.65}Nb_{0.35}O_4]$. The Raman spectra of the title compounds fit well into the series of the already known $Ge_9$-containing species and exhibit a very strong breathing mode at *ca.* 221 $cm^{-1}$ ($n_2$, $A_1$), the position of which is virtually constant, i.e., independent from the nature of the counterions and the environment, as well as characteristic bands at around 164 and 194 $cm^{-1}$.[25a,32] An intense low-range peak at 55 $cm^{-1}$ (compounds **3** and **4**) has been observed for the first time in compounds containing $Ge_9$ clusters. The peaks assigned to the $WO_4^{2-}$ and $NbO_4^{3-}$ anions are in good agreement with those reported in the literature.[33] Hence, the Raman spectra with very specific intensity patterns and characteristic wave numbers also confirm the presence of the different anions $[Ge_9]^{4-}$ and $WO_4^{2-}$ in the structures of **2**, **3**, **4** and of the anion $NbO_4^{3-}$ in the structure of **2**.

## ■ CONCLUSION

The most common way toward crystalline products containing group 14 element clusters is the extraction of binary or ternary alloys with ethylenediamine followed by the addition of the cation-sequestering agents [2.2.2]crypt or 18-crown-6.[34,35] Only a few examples show that crystalline products can be obtained from solution without such sequestering agents like the solvated phase $Rb_4[Ge_9][en]$, which crystallizes in a hierarchical derivative of the $Al_4YbMo_2$ structure type.[36] The use of salt melts instead of organic solvents as reaction media for Zintl anions was one of the basic ideas behind the investigation of mixed salts with Zintl anions. The existence of the composite compounds $A_{10+x}[Ge_9]_2[MO_4]$ shows that the inclusion of transition metal oxometallates into the structure of the almost genuine binary intermetallic phases $A_4Ge_9$ is possible.

The phases $A_{10+x}[Ge_9]_2[W_{1-x}Nb_xO_4]$ (A = K, Rb; $x$ = 0, 0.35) represent an interesting new class of materials in which an oxometallate anion with unfilled nonbonding states ($W^{6+}$ and $Nb^{5+}$, $d^0$) coexists with polynuclear units of a semimetal (Ge) in its negative oxidation state. It is well established that such Zintl


dx.doi.org/10.1021/ic202234b | *Inorg. Chem.* 2012, 51, 4058−4065

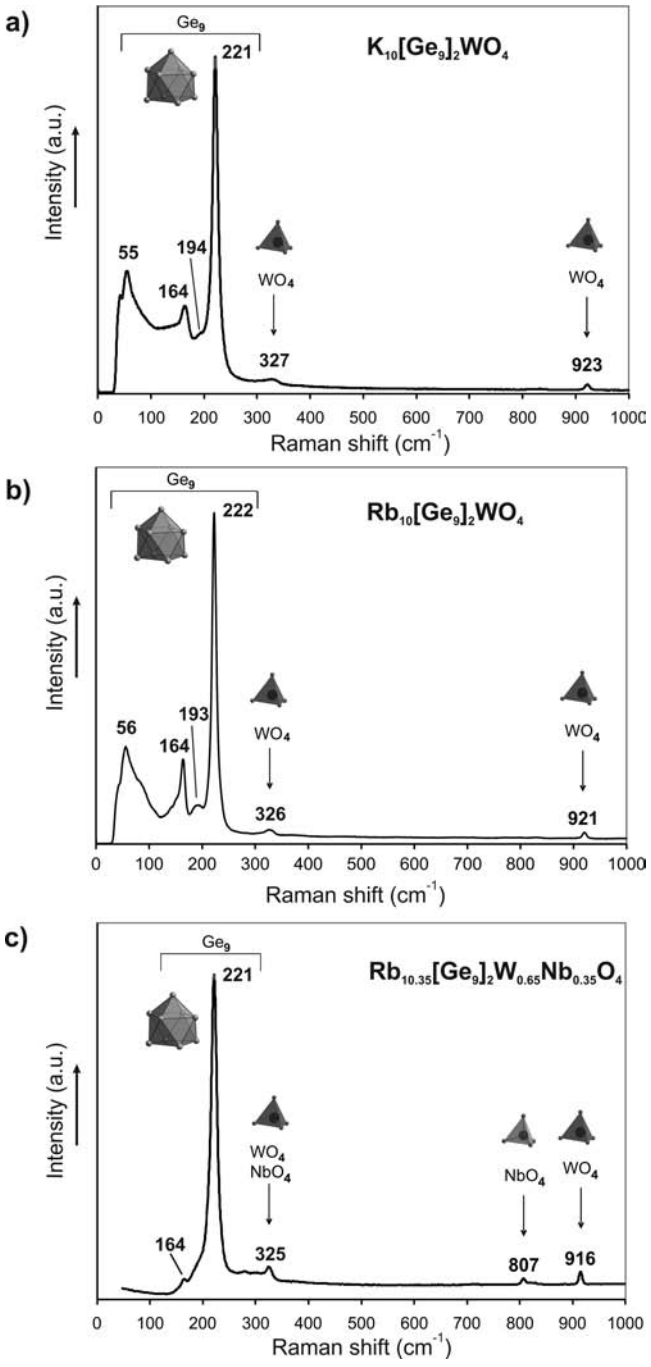


**Figure 5.** Raman spectra obtained from the single crystals of the mixed salts (a) $K_{10}[Ge_9]_2WO_4$, (b) $Rb_{10}[Ge_9]_2WO_4$, and (c) $Rb_{10.35}[Ge_9]_2W_{0.65}Nb_{0.35}O_4$.

anions can very easily be oxidized,[10] and this may be the main reason for their air- and moisture-sensitivity. The characterization of this new class of mixed salts involving Zintl anions and oxo-bonded transition metals clearly shows that the transition from semiconducting, salt-like Zintl phases to insulating salts is possible. The Zintl concept is retained in the Zintl-phase type structure part and can thus be used for the rational design of new classes of hybrid compounds with high application potential in fields like nanoscale materials or electro-optics. The most common approach to purely inorganic composite materials is the epitaxial fusion of two or more chemically distinct inorganic components as found in multi-component heterostructured nanoparticles.[2,3] Thus, the synthesis of the title compounds is a good example for crystal-engineered *all inorganic* composite materials. The next logical step is the search for double salts with other transition metal oxometallates such as $M^{5+}$ ($d^0$). First results including $Cs_{10}[Ge_9]_2[WO_4]$ and $Cs_{11}[Ge_9]_2[VO_4]$ have been very recently published in an independent report.[27]

## ■ ASSOCIATED CONTENT

### Ⓢ Supporting Information

Files containing detailed crystallographic data of crystals of $K_{10.35}W_{0.65}Ge_{18}Nb_{0.35}O_4$ (**1**), $Rb_{10.35}Ge_{18}W_{0.65}Nb_{0.35}O_4$ (**2**), $K_{10}Ge_{18}WO_4$ (**3**), and $Rb_{10}Ge_{18}WO_4$ (**4**) in CIF format as well as a collective CIF file of crystallographic data including further split positions of the Ge atoms for cluster **B** in **1**, **2**, and **4**; a figure of the split-atom model for K atoms around $W_{1-x}Nb_xO_4$ tetrahedra in **1** (Figure S1); figures of the X-ray powder patterns of $K_{10}[Ge_9]_2[WO_4]$ and $Rb_{10}[Ge_9]_2[WO_4]$ (Figures S2 and S3, respectively); a figure of the $Ge_9$ clusters in **1** and **2** (Figure S4) with bond labels in four groups (I, II, III, IV); a list of geometrical parameters of $Ge_9$ clusters in **1** and **2** (Table S1); lists of atomic and isotropic displacement parameters (Tables S2, S4, S5, S7, S9, S10, S12) as well as interatomic distances (Tables S3, S6, S8, S11) for compounds **1**, **2**, **3**, and **4**. This material is available free of charge via the Internet at http://pubs.acs.org.

## ■ AUTHOR INFORMATION

### Corresponding Author

*E-mail: thomas.faessler@lrz.tu-muenchen.de.

### Notes

The authors declare no competing financial interest.

## ■ ACKNOWLEDGMENTS

This work was supported by the European Union within the RTN program (EU-project Nr. HPRN-CT 2002-00193). The authors thank Prof. Lars Kloo and Dr. Martin Lindsjö of the KTH, Stockholm (Sweden), for Raman spectroscopy measurement and Dr. A. Schier for revising the manuscript.

## ■ REFERENCES

(1) Coronado, E.; Day, P. *Chem. Rev.* **2004**, *104* (11), 5419–5448.
(2) Jun, Y.-W.; Choi, J.-S.; Cheon, J. *Chem. Commun.* **2007**, 1203–1214.
(3) (a) Cheon, J.; Park, J.-I.; Choi, J.-S.; Jun, Y.-W.; Kim, S.; Kim, M. G.; Kim, Y.-M.; Kim, Y. J. *Proc. Natl. Acad. Sci. U.S.A.* **2006**, *103* (9), 3023–3027. (b) Kwon, K.-W.; Lee, B. H.; Shim, M. *Chem. Mater.* **2006**, *18*, 6357–6363.
(4) (a) Wengert, S.; Nesper, R. *J. Solid State Chem.* **2000**, *152*, 460–465. (b) Wengert, S.; Nesper, R.; Willems, J. B. *Chem.—Eur. J.* **2001**, *7* (15), 3209–3213.
(5) (a) Hoch, C.; Röhr, C. *Z. Naturforsch.* **2001**, *B56*, 423–430. (b) Hoch, C.; Röhr, C. *Z. Anorg. Allg. Chem.* **2002**, *628*, 1541–1548.
(6) Frisch, G.; Hoch, C.; Röhr, C.; Zönnchen, P.; Becker, K. D.; Niemeier, D. *Z. Anorg. Allg. Chem.* **2003**, *629*, 1661–1672. Wendorff, M.; Röhr, C. *Z. Anorg. Allg. Chem.* **2006**, *632*, 1792–1798.
(7) (a) Saltykov, V.; Nuss, J.; Jansen, M. *Z. Anorg. Allg. Chem.* **2011**, *637*, 1163–1168. (b) Saltykov, V.; Nuss, J.; Wedig, U.; Prasad, D. L. V. K.; Jansen, M. *Z. Anorg. Allg. Chem.* **2011**, *637*, 834–839. (c) Wedig, U.; Saltykov, V.; Nuss, J.; Jansen, M. *J. Am. Chem. Soc.* **2010**, *132*, 12458–12461.
(8) Hoffmann, S.; Fässler, T. F.; Hoch, C.; Röhr, C. *Angew. Chem.* **2001**, *113*, 4527–4529; *Angew. Chem., Int. Ed.* **2001**, *40*, 4398–4400.

(9) (a) Mudring, A. V.; Jansen, M. *Angew. Chem.* **2000**, *112*, 3194–3196; *Angew. Chem., Int. Ed.* **2000**, *39*, 3066–3067. (b) Mudring, A. V.; Nuss, J.; Wedig, U.; Jansen, M. *J. Solid State Chem.* **2000**, *155*, 29–36.
(10) Guloy, A. M.; Ramlau, R.; Tang, Z.; Schnelle, W.; Baitinger, M.; Grin, Y. *Nature* **2006**, *443*, 320–323.
(11) (a) Armatas, G. S.; Kanatzidis, M. G. *Nature* **2006**, *441*, 1122–1125. (b) Sun, D.; Riley, A. E.; Cadby, A. J.; Richmann, E. K.; Korlann, S. D.; Tolbert, S. H. *Nature* **2006**, *441*, 1126–1130.
(12) Fässler, T. F. *Coord. Chem. Rev.* **2001**, *215*, 347–377.
(13) Scharfe, S.; Kraus, F.; Stegmaier, S.; Schier, A.; Fässler, T. F. *Angew. Chem., Int. Ed.* **2011**, *50*, 3630–3670.
(14) Nienhaus, A.; Hauptmann, R.; Fässler, T. F. *Angew. Chem., Int. Ed.* **2002**, *41*, 3213–3215.
(15) (a) Xu, L.; Sevov, S. C. *J. Am. Chem. Soc.* **1999**, *121*, 9245–9246. (b) Ugrinov, A.; Sevov, S. C. *J. Am. Chem. Soc.* **2002**, *124*, 10990–10991. (c) Ugrinov, A.; Sevov, S. C. *Inorg. Chem.* **2003**, *42*, 5789–5791. (d) Downie, C.; Tang, Z.; Guloy, A. M. *Angew.Chem. Int. Ed.* **2000**, *39*, 337–340.
(16) (a) Hauptmann, R.; Fässler, T. F. *Z. Anorg. Allg. Chem.* **2003**, *629*, 2266–2273. (b) Yong, L.; Hoffmann, S. D.; Fässler, T. F. *Z. Anorg. Allg. Chem.* **2005**, *631*, 1149–1153. (c) Nienhaus, A.; Hoffmann, S. D.; Fässler, T. F. *Z. Anorg. Allg. Chem.* **2006**, *632*, 1752–1758.
(17) (a) Grandqvist, C. G. *Handbook of Inorganic Electrochromic Materials*; Elsevier: Amsterdam, 1995. (b) *Large Area Chromogenics: Materials and Devices for Transmittance Control*; Lampert, C. M., Grandqvist, C. G., Eds.; SPIE Press: Bellingham, WA, 1988; Vol. *IS4*.
(18) Koltypin, Yu.; Nikitenko, S. I.; Gedanken, A. *J. Mater. Chem.* **2002**, *12*, 1107–1110.
(19) (a) Aird, A.; Domeneghetti, M. C.; Mazzi, F.; Tazzoli, V.; Salje, E. K. H. *J. Phys.: Condens. Matter* **1998**, *10*, L569. (b) Polaczek, A.; Pekata, M.; Obuszko, Z. *J. Phys.: Condens. Matter* **1994**, *6*, 7909–7919.
(20) (a) Koesters, M.; Sturman, B.; Werheit, P.; Haertle, D.; Buse, K. *Nat. Photonics* **2009**, *3* (9), 510–513. (b) Dunn, M. H.; Ebrahimzadeh, M. *Science* **1999**, *286*, 1513–1517.
(21) (a) *X-RED32*, version 1.48; Stoe & Cie GmbH: Darmstadt, Germany, 2008. (b) *X-SHAPE*, version 2.11; STOE & Cie GmbH: Darmstadt, Germany, 2008.
(22) (a) Sheldrick, G. M. *SHELXS-97*; Universität Göttingen: Göttingen, Germany, 1997. (b) Sheldrick, G. M. *SHELXL-97*; Universität Göttingen: Göttingen, Germany, 1997.
(23) Fässler, T. F.; Hunziker, M.; Spahr, M. E.; Lueken, H.; Schilder., H. *Z. Anorg. Allg. Chem.* **2000**, *620*, 692–700.
(24) Ponou, S.; Fässler, T. F. *Z. Anorg. Allg. Chem.* **2007**, *633*, 393–397.
(25) (a) Carrillo-Cabrera, W.; Cardoso Gil, R.; Somer, M.; Persil, O.; von Schnering, H. G. *Z. Anorg. Allg. Chem.* **2003**, *629*, 601–608. (b) Hoch, C.; Wendorff, M.; Röhr, C. *Z. Anorg. Allg. Chem.* **2003**, *629*, 2391–2397. (c) Hoch, C.; Wendorff, M.; Röhr. *J. Alloys Compd.* **2003**, *361*, 206–221.
(26) Quenéau, V.; Sevov, S. C. *Angew. Chem.* **1997**, *109*, 1818–1820. *Angew. Chem., Int. Ed. Engl.* **1997**, *36*, 1754–1756.
(27) Hlukhyy, V.; Fässler, T. F. *Angew. Chem., Int. Ed.* **2012**, *51*, 742–747.
(28) (a) Kools, F. X. N. M.; Koster, A. S.; Rieck, G. D. *Acta Crystallogr.* **1969**, *B25*, 1704–1708. (b) Kools, F. X. N. M.; Koster, A. S.; Rieck, G. D. *Acta Crystallogr.* **1970**, *B26*, 1974–1977.
(29) *Inorganic Crystal Structure Database* [CD-Rom], version 1.4.6, Release 2009/2; Fachinformationszentrum Karlsruhe: Karlsruhe, Germany.
(30) Havinga, E. E.; Damsma, H.; Hokkeling, P. *J. Less-Common Met.* **1972**, *27*, 169–186.
(31) (a) For the tetrelide-tetrelate $V(Rb_{14}[Si_6O_{17}][Ge_9]) = 922$ Å$^3$ > $V(Rb_{10}[Si_6O_{17}]) + V(Rb_4[Ge_9]) = 885$ Å$^3$. (b) Hoffmann, S.; Fässler, T. F. *Inorg. Chem.* **2006**, *45*, 7968–7972.
(32) (a) von Schnering, H. G.; Baitinger, M.; Bolle, U.; Carrillo-Cabrera, W.; Curda, J.; Grin, Y.; Heinemann, F.; Llanos, J.; Peters, K.; Somer, M. *Z. Anorg. Allg. Chem.* **1997**, *623*, 1037–1039. (b) Carrillo-Cabrera, W.; Aydemir, U.; Somer, M.; Kircali, A.; Fässler, T. F.; Hoffmann., S. D. *Z. Anorg. Allg. Chem.* **2007**, *633*, 1575–1580.
(33) (a) Weinstock, N.; Schulze, H.; Müller, A. *J. Chem. Phys.* **1973**, *59* (9), 5063. (b) Nagarathna, H. M.; Bencivenni, L.; Gingerich, K. A. *J. Chem. Phys.* **1984**, *81* (2), 591–598. (c) Pradhan, A. K.; Choudhary, R. N. P. *Phys. Status Solidi* **1987**, *143(b)*, K161–K166.
(34) Fässler, T. F.; Hoffmann, R. *J. Chem. Soc., Dalton Trans.* **1999**, 3339–3340.
(35) Corbett, J. D.; Edwards, P. A. *J. Am. Chem. Soc.* **1977**, *99*, 3313–3317.
(36) Somer, M.; Carrillo-Cabrera, W.; Peters, E. M.; Peters, K.; von Schnering, H. G. *Z. Anorg. Allg. Chem.* **1998**, *624*, 1915–1921.